European Journal of Radiology Open 8 (2021) 100327

Contents lists available at ScienceDirect

European Journal of Radiology Open

journal homepage: www.elsevier.com/locate/ejro

Impact of different phased-array coils on the quality of prostate magnetic resonance images

Daniel Stocker [a], Andrei Manoliu [a,b,c,d], Anton S. Becker [a], Borna K. Barth [a], Daniel Nanz [a,e], Markus Klarhöfer [f], Olivio F. Donati [a,*]

[a] Institute of Diagnostic and Interventional Radiology, University Hospital Zurich and University of Zurich, Switzerland
[b] Max-Planck UCL Centre for Computational Psychiatry and Ageing Research, London, UK
[c] Wellcome Trust Centre for Human Neuroimaging, UCL, London, UK
[d] Psychiatric University Hospital, University of Zurich, Switzerland
[e] Swiss Center for Musculoskeletal Imaging, SCMI, Balgrist Campus AG, Switzerland and Medical Faculty, University of Zurich, Zurich, Switzerland
[f] Siemens Healthcare AG, Zurich, Switzerland

HIGHLIGHTS

- Image quality is similar for different body phased-array receive coil setups.
- An 18-channel body phased-array receive coil setup achieved good image quality.
- 60-channel body phased-array receive coil setup slightly improves SNR in T2W images.

ARTICLE INFO

Keywords:
Magnetic resonance imaging
Prostate imaging
Signal-to-noise ratio

ABSTRACT

Purpose: To evaluate the influence of body phased-array (BPA) receive coil setups on signal-to-noise ratio (SNR) and image quality (IQ) in prostate MRI.
Methods: This prospective study evaluated axial T2-weighted images (T2W-TSE) and DWI of the prostate in ten healthy volunteers with 18-channel (18CH), 30-channel and 60-channel (60CH) BPA receive coil setups. SNR and ADC values were assessed in the peripheral and transition zones (TZ). Two radiologists rated IQ features. Differences in qualitative and quantitative image features between BPA receive coil setups were compared. After correction for multiple comparisons, p-values <0.004 for quantitative and p-values <0.017 for qualitative image analysis were considered statistically significant.
Results: Significantly higher SNR was found in T2W-TSE images in the TZ using 60CH BPA compared to 18CH BPA coil setups (15.20 ± 4.22 vs. 7.68 ± 2.37; $p = 0.001$). There were no significant differences between all other quantitative (T2W-TSE, $p = 0.007-0.308$; DWI, $p = 0.024-0.574$) and qualitative image features (T2W-TSE, $p = 0.083-1.0$; DWI, $p = 0.046-1.0$).
Conclusion: 60CH BPA receive coil setup showed marginal SNR improvement in T2W-TSE images. Good IQ could be achieved with 18CH BPA coil setups.

1. Introduction

In recent years, multi-parametric prostate magnetic resonance imaging (mpMRI) has become the predominant imaging modality for detection and characterization of cancer foci in patients with suspected prostate cancer [1–5]. mpMRI of the prostate in such patients

Abbreviations: 18CH, BPA 18-channel body array coil; 30CH, BPA 30-channel body array coil; 60CH, BPA 60-channel body array coil; ANOVA, Analysis of variances; BPA, Body phased-array; ERC, Endorectal coil; ICC, Intra-class correlation coefficient; IQR, Interquartile range; mpMRI, Multi-parametric magnetic resonance imaging; PSTT, Post-hoc paired-sample t-tests; ROIs, Region of interests; SD, Standard deviation; SNR, Signal to noise ratio; ss-DWI-EPI, Single-shot diffusion-weighting spin-echo echo-planar imaging; T2W-TSE, T2-weighted turbo spin echo.

* Corresponding author at: Institute of Diagnostic and Interventional Radiology, University Hospital Zurich, Rämistrasse 100, CH-8091, Zurich, Switzerland.
E-mail address: olivio.donati@usz.ch (O.F. Donati).

https://doi.org/10.1016/j.ejro.2021.100327
Received 11 January 2021; Received in revised form 21 January 2021; Accepted 21 January 2021

significantly reduces the number of unnecessary transrectal ultrasound-guided biopsies [6–9].

An important step towards increasing patients' acceptance for mpMRI of the prostate is obviating the use of an endorectal coil (ERC) for signal reception while maintaining good image quality for the detection of prostate cancer [10]. Previous studies have demonstrated comparable image quality in mpMRI of the prostate with and without the use of an ERC, while increasing patient comfort in examinations without using an ERC [11,12]. Regardless of whether or not an ERC is used, one or more body phased-array receive coils (BPA) with typically 8–32 channels are used in mpMRI of the prostate [11–16]. While the effect of image quality using BPAs with a high number of channels was tested in other body parts [17–22], the influence of different BPAs on the image quality in mpMRI of the prostate has only been evaluated in one study [23], showing improved performance of 32 compared to 12 independent receiver coils.

The coil elements within BPAs are connected to a variable number of independent receive channels on the MRI-scanner. Multiple coil elements may increase signal to noise ratio (SNR) in parallel imaging [24,25]. While coils allowing for high acceleration factors and therefore reducing acquisition time [16] are often used for brain imaging, such coils with high channel density were only recently introduced for body imaging.

Thus, the purpose of our study was to evaluate the influence of different BPA setups on the SNR, geometric distortion and image quality in mpMRI of the prostate.

2. Material and methods

This prospective study was approved by the regional ethics committee. Written informed consent was obtained from all volunteers.

2.1. Study population

Ten healthy volunteers (mean age 26.1 ± 3.8 years; BMI 23.2 ± 3.0 kg/m^2) underwent an adapted prostate MRI-protocol at one timepoint. Volunteers older than 18 years, without contraindications for MR-scanning and without known focal prostate lesion were included.

2.2. MRI technique

No instructions with regards to clearing rectal gas were given before the MRI.

All images were acquired on a 3 T MRI system (MAGNETOM Skyra, Siemens Healthcare, Erlangen, Germany) using two independent transmit channels (TimTX TrueShape, Siemens Healthcare, Erlangen, Germany). For signal reception, all ten volunteers were examined with three different BPA receive coil setups in random order: 1) 8 elements of a 32-channel spine coil (Spine 32, Siemens Healthcare, Erlangen, Germany) integrated in the MR table and covering the pelvis posteriorly and 12 elements of an 18-channel body array coil (Body 18, Siemens Healthcare, Erlangen, Germany) covering the pelvis anteriorly (hereafter referred to as 18CH BPA coil); 2) 8 elements of a 32-channel spine coil (Spine 32, Siemens Healthcare, Erlangen, Germany) covering the pelvis posteriorly and 20 elements of a 30-channel body array coil (Body 30, Siemens Healthcare, Erlangen, Germany) coil covering the pelvis anteriorly (hereafter referred to as 30CH BPA coil); 3) a 60-channel BPA coil setup consisting of an anterior and posterior 30CH phased-array coil (Body 30, Siemens Healthcare, Erlangen, Germany), covering the pelvis from both sides (hereafter referred to as 60CH BPA coil).

The 18CH phased-array coil consists of 18 elements arranged in 3 rows of 6 elements, while each of the 30CH phased-array coils consist of 30 elements arranged in three rows of 10 elements each.

Axial T2-weighted turbo spin echo (T2W-TSE) sequences were acquired with repetition time (TR) / echo time (TE) 6650 / 96 ms; FoV 222 × 222 mm^2, slice thickness (ST) 3 mm and in-plane resolution 0.5 × 0.5 mm^2; 2 averages; acquisition time 4 min and 49 s.

Single-shot diffusion-weighting spin-echo echo-planar imaging (ss-DWI-EPI) sequences were acquired with orientation and location identical to T2W-TSE images. Acquisition parameters for ss-DWI-EPI were: TR / TE 4600 / 68 ms, receiver bandwidth 1526 Hz/Px; b-values 100, 500, and 1000s/mm^2; FOV 222 × 222 mm^2, ST 3 mm; in-plane resolution 1.8 × 1.8 mm^2; parallel imaging (GRAPPA) with acceleration factor 2; acquisition time 5 min and 42 s.

All parameters were kept identical while using the different phased-array receive coil setups. ADC maps were calculated for each DWI sequence with a monoexponential fit based on the three measured b-values.

2.2.1. SNR measurements and analysis

SNR analysis followed the procedure described by [26–29], which has previously been applied for SNR evaluation of prostate MRI [29]. Briefly, we acquired all T2W-TSE and b-100 DWI-sequences twice (two T2W-TSE back-to-back and two b-100 DWI back-to-back) and calculated subtraction images. Subsequently, one noise-map for each set of sequences was created and SNR was calculated as follows:

$$SNR = \frac{|\rho|}{\sigma} \times \sqrt{2}$$

where ρ is the measured image intensity, proportional to the magnitude of the measured transverse magnetization, σ is the standard deviation of the corresponding noise components as measured on the difference image, and $\sqrt{2}$ is a correction factor [26,27]. Voxel-wise SNR-maps were calculated by post-processing image data and corresponding noise data separately. Regions of interest (ROIs) were placed within the left and right peripheral zone as well as within the transition zone of the prostate by one radiologist (A.M., 4 years of experience in cross-sectional imaging) who was not involved in the qualitative readout. Mean SNR-values of these ROIs were extracted and SNR-values within the left and right peripheral zone were averaged for further analysis. An example of SNR maps for all BPA coil setups for T2W-TSE and DWI sequences is presented in Fig. 1.

2.2.2. ADC measurements and analysis

Circular ROIs were placed on each side of the transition zone and the peripheral zone. Mean ADC-value for each ROI in the left and right transition and peripheral zones were extracted separately. For further statistical analysis ADC-values for the left and right peripheral zone as well as for the left and right transition zone were averaged.

2.2.3. Geometric distortion

For the evaluation of geometric distortion, we measured the prostate diameters from anterior to posterior and from left to right at the level of the verumontanum on all different b-1000 DWI-images as well as all different T2W-TSE images. Measurements were conducted using a commercially available DICOM viewer (Osirix®, version 5.9; The OsiriX Foundation, Geneva, Switzerland). For subsequent statistical analysis we assessed diameter differences between DWI and T2W-TSE images. The measurements on the T2W-TSE images were used as standard of reference for the definition of anatomic borders.

2.3. Qualitative image analysis

The T2W-TSE images and the b-1000 DWI images of all volunteers were independently reviewed by two radiologists (A.S.B. and B.K.B, both with 3 years of experience in interpreting prostate MRI) blinded to the coil used. T2W-TSE images and the DWI were arranged in random order and reviewed in one reading session. A 5-point Likert scale was used to evaluate different image quality parameters such as resolution, demarcation of prostate capsule, zonal anatomy, and overall image quality (1, poor; 2, impaired; 3, acceptable; 4, good; 5, excellent)

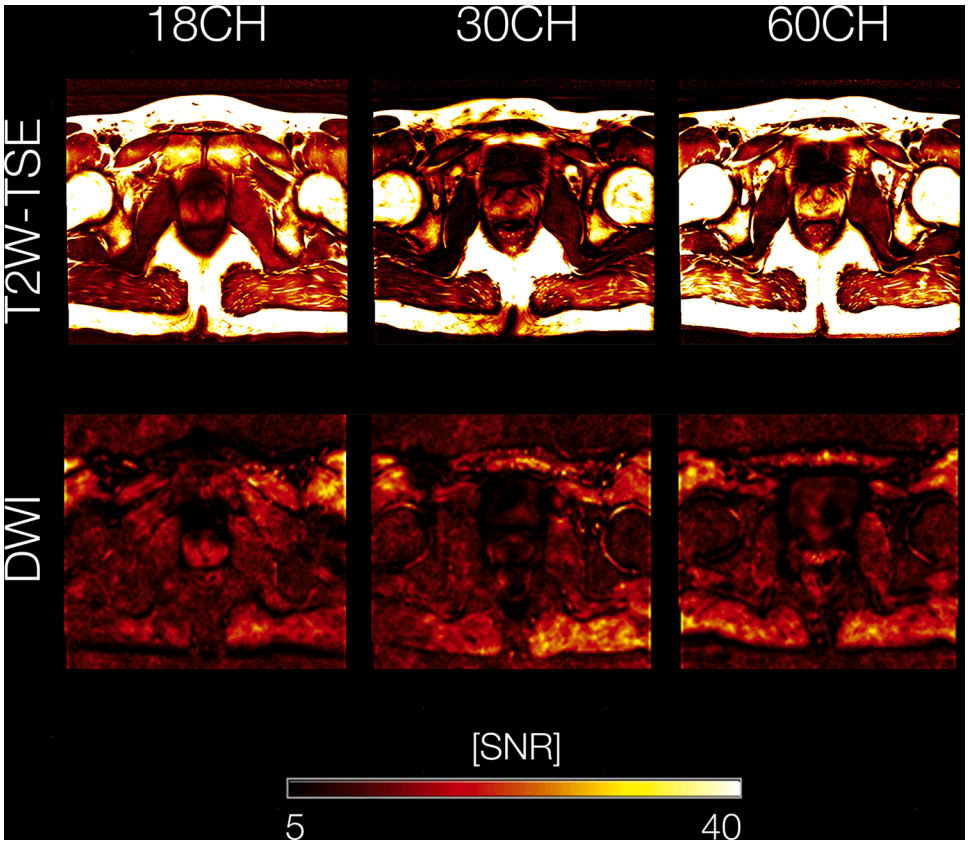

Fig. 1. Voxel-wise SNR maps for a representative participant. T2W-TSE and DWI images were postprocessed individually together with the corresponding noise data, yielding SNR maps on a voxel-wise basis. SNR maps are shown for T2W-TSE / DWI sequences using 18CH, 30CH as well as 60CH coils, respectively. SNR values are color-coded from 5 (black) to 40 (yellow/white). (For interpretation of the references to colour in this figure legend, the reader is referred to the web version of this article).
Abbreviations: SNR, signal-to-noise ratio; T2W-TSE, T2-weighted turbo spin echo; DWI, diffusion weighted images; 18CH, 18-channel body phased-array receive coil setup; 30CH, 30-channel body phased-array receive coil setup; 60CH, 60-channel body phased-array receive coil setup.

separately as previously reported [29]. Additionally, we evaluated geometric distortion (1, no distortion; 2, low distortion; 3, intermediate distortion; 4, high distortion; 5, very high distortion, respectively) on DWI and the clarity of the periurethral region on T2W-TSE images. Also, the presence of artifacts in the DWI-sequences (wrapping, ghosting, susceptibility, blurring and other) and their influence on image quality and on the diagnostic evaluation, using a 5-point Likert scale (1, no influence; 2, low influence; 3, moderate influence; 4, severe influence; 5, substantial influence, respectively) were assessed. Furthermore, the readers had to state whether the image series were diagnostic or not. At the end of the reading session, the three different T2W-TSE image series for each volunteer were presented to the reader side-by-side and they were asked to choose their overall preferred sequence.

2.4. Statistical analysis

Significant differences for qualitative image features between the three different phased-array receive coil setups for the T2W-TSE images and the DWI were evaluated using the Wilcoxon rank sum tests with Bonferroni correction for multiple comparisons. For the analysis of quantitative measurements of SNR and ADC, we performed an analysis of variances (ANOVA) to test for potential group interactions with respect to measured values within the peripheral and transition zone of the prostate. Post-hoc paired-sample t-tests (PSTT) were performed to identify potential differences in SNR and ADC between each pair of phased-array receive coil setups. Significant differences in quantitative analysis of geometric distortion were evaluated using Friedman tests. After correction for multiple comparisons p-values <0.0042 for the quantitative image analysis (Benjamini-Hochberg procedure, $n = 12$ to account for all performed PSTT) and p-values <0.017 for the qualitative image analysis (Bonferroni correction, $n = 3$ to account for all body phased-array receive coil setups) were considered statistically significant, respectively. All tests were two-tailed. We used the intra-class correlation coefficient (ICC) to assess inter-reader agreements for all qualitative image features. An ICC of 0.75–1.00 indicated excellent, 0.60−0.74 good, 0.40−0.59 fair and <0.4 poor agreement [30]. All statistical analyses were performed using SPSS (IBM® SPSS® Statistics 22; SPSS® Inc., Chicago, IL) and R (v3.3.1. The R Foundation for Statistical Software, Vienna, Austria).

3. Results

3.1. Quantitative analysis

With respect to the T2W-TSE images, the signal-to-noise ratio (SNR; mean ± SD for the peripheral / transition zone within the prostate) was 18.16 ± 6.04 / 7.68 ± 2.37 for the 18CH BPA coil, 22.45 ± 4.52 / 11.54 ± 4.44 for the 30CH BPA coil, and 24.61 ± 5.62 / 15.20 ± 4.22 for the 60CH BPA coil, respectively. The ANOVA showed a statistically significant group-effect in the transition zone ($F = 7.879$, $p < 0.001$) but not in the peripheral zone ($F = 2.929$, $p = 0.024$). Post-hoc paired-sample t-tests revealed higher SNR in the transition zone when using the 60CH BPA coil compared to the 18CH BPA coil ($T=-4.965$, $p = 0.001$,), but not for other coil comparisons or regions of the prostate (see also Table 1 for detailed presentation of corresponding values). Regarding the DWI images, SNR was 17.32 ± 4.24 / 11.43 ± 2.44 for the 18CH BPA coil, 16.09 ± 5.95 / 10.47 ± 2.02 for the 30CH BPA coil, and 30.24 ± 15.45 / 15.19 ± 4.32 for the 60CH BPA coil. ANOVA as well as post-hoc paired-sample t-tests did not reveal statistically significant differences in SNR between all BPA coils in both the peripheral and transition zone (Table 1).

ADC (mean ± SD for the peripheral / transition zone within the prostate) was $1078 \pm 127.09 \times 10^{-6}$ mm^2/ $960.7 \pm 118.5 \times 10^{-6}$ mm^2 for the 18CH BPA coil, $1148 \pm 272.5 \times 10^{-6}$ mm^2 / $1078.5 \pm 168.9 \times 10^{-6}$ mm^2 for the 30CH BPA coil, and $1060.3 \pm 134.8 \times 10^{-6}$ mm^2 / $1008.8 \pm 127.4 \times 10^{-6}$ mm^2 for the

Table 1
Signal-to-noise ratio analysis. To evaluate potential differences between pairs of phased array receive coil setups in SNR within the peripheral and transition zone of the prostate for T2-weighted turbo spin echo and diffusion weighted images, post-hoc paired-sample t-tests (PSTT) were performed. After correction for multiple comparisons (Benjamini-Hochberg procedure, n = 12 to account for all performed PSTT) a p-value <0.004 was considered statistically significant. Italics indicate p-values <0.004.

		Peripheral Zone			Transition Zone		
		SNR	T-value	p-value	SNR	T-value	p-value
T2W-TSE	**18CH vs. 30CH**	18.16 ± 6.04 vs. 22.45 ± 4.52	−2.182	0.061	7.68 ± 2.37 vs. 11.54 ± 4.44	−3.623	0.007
	18CH vs. 60CH	18.16 ± 6.04 vs. 24.61 ± 5.62	−1.983	0.083	7.68 ± 2.37 vs. 15.20 ± 4.22	−4.965	*0.001*
	30CH vs. 60CH	22.45 ± 4.52 vs. 24.61 ± 5.62	−1.089	0.308	11.54 ± 4.44 vs. 15.20 ± 4.22	−2.166	0.062
DWI	**18CH vs. 30CH**	17.32 ± 4.24 vs. 16.09 ± 5.95	0.586	0.574	11.43 ± 2.44 vs. 10.47 ± 2.02	0.940	0.375
	18CH vs. 60CH	17.32 ± 4.24 vs. 30.24 ± 15.45	−2.626	0.030	11.43 ± 2.44 vs. 15.19 ± 4.32	−2.434	0.041
	30CH vs. 60CH	16.09 ± 5.95 vs. 30.24 ± 15.45	−2.782	0.024	10.47 ± 2.02 vs. 15.19 ± 4.32	−2.770	0.024

Abbreviations: SNR, signal-to-noise ratio; T2W-TSE, T2-weighted turbo spin echo; DWI, diffusion weighted images; 18CH, 18-channel body phased-array receive coil setup; 30CH, 30-channel body phased-array receive coil setup; 60CH, 60-channel body phased-array receive coil setup.

60CH BPA coil, respectively. The ANOVA showed no statistically significant group effect in the peripheral zone (F = 0.594, p = 0.559) and the transition zone (F = 1.790, p = 0.186). Also, the post-hoc paired-sample t-tests revealed no significant difference between the three different BPA receive coils in both, the peripheral (p = 0.936–1.0) and the transition zone (p = 0.212–1.0). Boxplots for ADC measurements are presented in Fig. 2.

There were no statistically significant differences in left to right and anterior to posterior diameter of the prostate between the DWI-sequences and the T2W-TSE sequences of all three different BPA coils (p = 0.905 and 0.836, respectively). The median diameter difference from left to right was 0.1 mm (interquartile range (IQR) −1.6 to 2.1 mm) and from anterior to posterior −0.5 mm (IQR −1.8 to 2.7 mm) for the 18CH BPA coil, -0.1 mm (IQR −2.1 to 0.9 mm) and 0.6 mm (IQR −1.6 to 2.4 mm) for the 30CH BPA coil and −0.5 mm (IQR −0.7 to 0.8 mm) and −0.6 (IQR −1.7 to 1.1 mm) for the 60CH BPA receive coil, respectively.

3.2. Qualitative analysis

The inter-reader agreement between reader 1 and reader 2 for the T2W-TSE sequences was excellent for resolution (ICC 0.839; 95 % confidence interval (95 % CI) 0.661 – 0.923), demarcation of the prostate capsule (ICC 0.828, 95 % CI 0.639 – 0.918), the clarity of the periurethral region (ICC 0.797, 95 % CI 0.573 – 0.903) and for overall image quality (ICC 0.841, 95 % CI 0.667 – 0.924) and good for zonal anatomy (ICC 0.710, 95 % CI 0.390 – 0.862). For the DWI-sequences the inter-reader agreement was excellent for the influence of artifacts on the image quality (ICC 0.798, 95 % CI 0.575 – 0.904) and the influence of artifacts on the diagnostic performance (ICC 0.951, 95 % CI 0.896 – 0.977) and good for resolution (ICC 0.647, 95 % CI 0.259 – 0.832), demarcation of the prostate capsule (ICC 0.724, 95 % CI 0.419 – 0.868), zonal anatomy (ICC 0.748, 95 % CI 0.470 – 0.880), geometric distortion (ICC 0.710, 95 % CI 0.392 – 0.862) and overall image quality (ICC 0.607, 95 % CI 0.174 – 0.813).

There was no significant difference between the 18CH, the 30CH and the 60CH BPA coil setups for all tested values in the T2W-TSE and the DWI sequences (p = 0.083–1.0 and p = 0.046–1.0, respectively). Reader 1 rated one T2W-TSE image series with the 30CH BPA coil setup as well as one image series of the DWI-sequence in each coil setup not diagnostic. Other than the aforementioned exceptions, all other image sets were rated as diagnostic for both readers. These qualitative results are summarized in Table 2 and an example of T2W-TSE and DWI is presented in Fig. 3.

On side-by-side comparison, the T2W-TSE from the 18CH BPA setup was most frequently selected as the preferred series by reader 1 (in n = 4 of 10 volunteers) while reader 2 selected the 18CH and the 30CH BPA setup most (in n = 4 of 10 volunteers each).

4. Discussion

Three different BPA receive coil setups for MRI of the prostate were investigated. We found a tendency towards better SNR with increasing number of coil elements in the T2W-TSE sequences. However, significantly higher SNR was only found in the transition zone in T2W-TSE images for the 60CH as compared to the 18CH BPA coil setup. Image quality in general was rated high by both readers and appearance of artifacts were similar in all images across the different coil setups with no relevant influence on the image quality or diagnostic evaluation. Furthermore, choice of coil setup did not influence quantitative measures, such as the ADC, which is important regarding the inclusion of such measures in further updated reporting guidelines or for conducting multicenter studies [31].

Theoretically, BPA receive coils cover a large FOV while maintaining a high SNR allowing for improved image quality and parallel imaging to reduce the acquisition time [24,25,32]. However, recently published studies in body [19] and brain MRI [20,33] showed that the improvement in SNR by using an increased number of coil elements is most distinct in sequences that use a high acceleration factor, due to the lower noise amplification. In our study we used an acceleration factor of 2 for

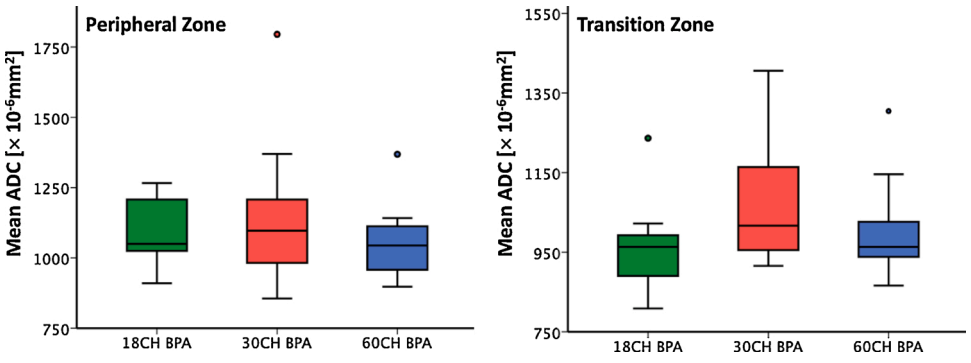

Fig. 2. Boxplots for ADC measurements in the peripheral and transition zone. ADC measurements in the peripheral and transition zone were similar between the 18CH BPA, 30CH BPA and 60CH BPA receive coil setup without significant differences between the coil setups (ANOVA peripheral zone F = 0.594, p = 0.55; transition zone F = 1.790, p = 0.186).
Abbreviation: ADC, apparent diffusion coefficient; 18CH BPA, 18-channel body phased-array receive coil setup; 30CH BPA, 30-channel body phased-array receive coil setup; 60CH BPA, 60-channel body phased-array receive coil setup; ANOVA, Analysis of variances.

Table 2
Qualitative results of conventional reading (Likert score ± standard deviation), number of artifacts, diagnostic sequences and results from Wilcoxon signed rank test. After correction for multiple comparisons (Bonferroni correction, n = 3 to account for all body phased-array receive coil setups) a p-value <0.017 was considered statistically significant.

		T2W-TSE			p-value			DWI			p-value		
		18CH	30CH	60CH	18CH vs. 30CH	18CH vs. 60CH	30CH vs. 60CH	18CH	30CH	60CH	18CH vs. 30CH	18CH vs. 60CH	30CH vs. 60CH
Resolution	R1	4.3 ± 0.7	3.9 ± 1.1	4.1 ± 0.7	0.102	0.414	0.527	4.1 ± 0.7	4.2 ± 0.6	4.2 ± 0.6	0.564	0.655	1
	R2	4.6 ± 0.7	4.4 ± 0.8	4.7 ± 0.5	0.414	0.655	0.317	4.4 ± 1.0	4.1 ± 0.9	4.3 ± 0.7	0.180	0.564	0.414
Capsule demarcation	R1	4.8 ± 0.4	4.4 ± 0.8	4.8 ± 0.4	0.102	1	0.102	4.7 ± 0.5	4.4 ± 1.0	4.5 ± 0.7	0.180	0.157	0.564
	R2	4.8 ± 0.4	4.6 ± 0.5	4.9 ± 0.3	0.157	0.564	0.083	4.8 ± 0.6	4.2 ± 0.9	4.6 ± 1.0	0.063	0.157	0.234
Zonal anatomy	R1	4.0 ± 0.8	3.9 ± 1.1	4.2 ± 0.8	0.705	0.480	0.257	4.2 ± 0.8	3.9 ± 0.7	3.8 ± 0.8	0.257	0.046	0.705
	R2	4.4 ± 0.7	4.6 ± 0.5	4.8 ± 0.4	0.317	0.102	0.480	4.6 ± 1.0	4.0 ± 1.2	4.3 ± 1.1	0.034	0.180	0.180
Overall IQ	R1	4.3 ± 0.7	4.3 ± 1.1	4.4 ± 0.7	1	0.564	0.655	4.2 ± 0.8	4.1 ± 0.7	3.9 ± 0.9	0.655	0.180	0.480
	R2	4.6 ± 0.7	4.3 ± 0.8	4.7 ± 0.5	0.180	0.655	0.102	4.4 ± 0.8	4.3 ± 0.7	4.5 ± 0.7	0.705	0.739	0.157
Periurethral clarity	R1	4.4 ± 0.7	4.3 ± 1.1	4.5 ± 0.7	0.739	0.655	0.317						
	R2	4.7 ± 0.5	4.7 ± 0.7	4.9 ± 0.3	1	0.317	0.414						
Geometric distortion	R1							1.6 ± 1.0	2.0 ± 1.1	1.7 ± 1.1	0.194	0.705	0.334
	R2							1.7 ± 0.9	1.7 ± 0.9	2.3 ± 1.6	1	0.131	0.206
Number of artifacts	R1							5	6	8	0.564	0.180	0.317
	R2							4	5	5	0.655	0.655	1
Artifacts influencing diagnostic evaluation	R1							1.3 ± 0.9	1.6 ± 1.1	1.4 ± 1.0	0.414	0.317	0.705
	R2							1.2 ± 0.6	1.5 ± 1.1	1.3 ± 0.9	0.180	0.317	0.317
Artifacts influencing IQ	R1							1.8 ± 1.2	2.2 ± 1.3	2 ± 0.8	0.336	0.414	0.739
	R2							1.6 ± 1.0	1.8 ± 1.0	1.7 ± 1.1	0.414	0.705	0.739
Diagnostic (yes/no)	R1	10/0	9/1	10/0	0.317	1	0.317	9/1	9/1	9/1	1	1	1
	R2	10/0	10/0	10/0	1	1	1	10/0	10/0	10/0	1	1	1

Abbreviations: T2W-TSE, T2-weighted turbo spin echo; DWI, diffusion weighted images; 18CH, 18-channel body phased-array receive coil setup; 30CH, 30-channel body phased-array receive coil setup; 60CH, 60-channel body phased-array receive coil setup; R1, reader 1; R2, reader 2; IQ, image quality.

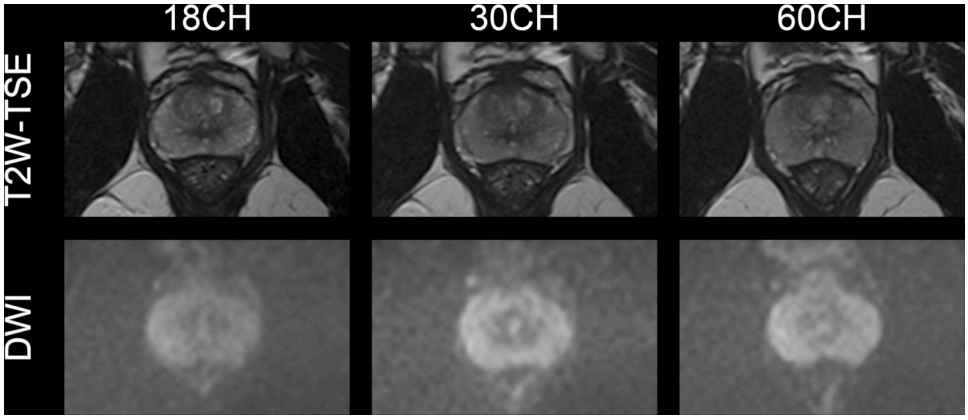

Fig. 3. Exemplary images acquired with three different coil setups in the same volunteer side-by-side. Images of the prostate at the midgland level of the T2W-TSE images from the 18CH, 30CH and 60CH coil setup and the DWI are shown. Qualitative image features for the different coil setups were rated with similar subjective scores for T2W-TSE and DWI. The overall image quality for the 18CH, 30CH and 60CH coil setup was rated 5, 5 and 5 for T2W-TSE images and 5, 4 and 4 for DWI by both readers. All T2W-TSE and DWI sequences were rated diagnostic by both readers.
Abbreviations: T2W-TSE, T2-weighted turbo spin echo; DWI, diffusion weighted images; 18CH, 18-channel body phased-array receive coil setup; 30CH, 30-channel body phased-array receive coil setup; 60CH, 60-channel body phased-array receive coil setup.

the DWI-sequence and no parallel imaging for the T2W-TSE sequence and no significantly better image quality was demonstrated by using the 60CH BPA coil setup. These results are in line with other studies comparing image quality in abdominal MRI when using low acceleration factors [19].

The 60CH BPA coil design, may potentially enable higher image quality for measurements where high acceleration factors are applied. While previous studies have shown a reduction of acquisition time in body MRI [34], in mpMRI of the prostate there is only a relatively small area to be covered with a limited number of transverse slices. Therefore, our data suggest that the benefits from the 60CH BPA coil design in mpMRI of the prostate remain questionable.

In multichannel coils, the gain of SNR is particularly high in areas close to the coil elements while decreasing with increasing depth, i.e. distance from the coil elements [33,35–38]. Our study results show a tendency towards higher SNR with increasing coil elements which may be related to the study population, consisting of young volunteers with a normal BMI. However, the differences in SNR may have reached significant levels in a larger study population, also including elderly men with higher BMI. However, it would have been difficult to perform multiple MR scans with different BPA coil setups in actual patients with suspicion for prostate cancer who undergo clinically indicated prostate

MRI with consistently high image quality throughout all scans. We believe that high quality images with high SNR can be achieved likewise with 18CH, 30CH and 60CH BPA coil setups.

Since geometric distortion is not dependent on the phased-array coils, there expectedly were no differences in geometric distortion between the three different coil setups. However, we chose to include evaluation for geometric distortion in T2W-TSE and DWI to ensure distortion free, high image quality in all image sets.

Our study has limitations. First, the sample size was relatively small, however, in the range of a typical volunteer study. Second, we did investigate young and healthy volunteers and not patients with suspicion of prostate cancer, hence tumor delineation and evaluation of conspicuity of suspicious lesions could not be evaluated. However due to the study design and given that the main focus was set on evaluation of image quality parameters, performing the study in patients clinically referred for a mpMRI of the prostate would not have been feasible due to a relatively long scan duration (including acquisition of multiple sequences using three different coil setups). Third, we did not investigate the influence of higher acceleration factors of the MRI-sequences on the SNR. However, the main goal in our study was to evaluate the influence of the number of coil elements on qualitative and quantitative image features in a typically used protocol of mpMRI of the prostate.

In conclusion, although the 60CH BPA receive coil setup showed a tendency towards higher SNR in T2W-TSE images and DWI compared to the 18CH BPA and 30CH BPA setup, there was no statistically significant difference between these coil setups regarding image quality or geometric distortion. Good image quality may be achieved with a typically used 18CH BPA coil setup.

Ethical statement

The regional ethics committee of Zurich, Switzerland (Kantonale Ethikkommission Zürich) approved this study. Written informed consent was obtained from all volunteers.

Funding statement

Andrei Manoliu received a grant from the swiss national science foundation (P2SKP3_178107).

CRediT authorship contribution statement

Daniel Stocker: Writing - original draft, Investigation, Data curation, Formal analysis, Visualization. **Andrei Manoliu:** Writing - review & editing, Data curation, Formal analysis, Visualization. **Anton S. Becker:** Investigation, Writing - review & editing, Formal analysis. **Borna K. Barth:** Investigation, Writing - review & editing. **Daniel Nanz:** Writing - review & editing. **Markus Klarhöfer:** Writing - review & editing. **Olivio F. Donati:** Conceptualization, Methodology, Writing - review & editing, Supervision, Project administration.

Declaration of Competing Interest

The authors declare that they have no known competing financial interests or personal relationships that could have appeared to influence the work reported in this paper.

References

[1] M. de Rooij, E.H. Hamoen, J.J. Futterer, J.O. Barentsz, M.M. Rovers, Accuracy of multiparametric MRI for prostate cancer detection: a meta-analysis, AJR Am. J. Roentgenol. 202 (2) (2014) 343–351.

[2] O.F. Donati, Y. Mazaheri, A. Afaq, H.A. Vargas, J. Zheng, C.S. Moskowitz, H. Hricak, O. Akin, Prostate cancer aggressiveness: assessment with whole-lesion histogram analysis of the apparent diffusion coefficient, Radiology 271 (1) (2014) 143–152.

[3] M. Sauer, J.M. Weinrich, C. Fraune, G. Salomon, P. Tennstedt, G. Adam, D. Beyersdorff, Accuracy of multiparametric MR imaging with PI-RADS V2 assessment in detecting infiltration of the neurovascular bundles prior to prostatectomy, Eur. J. Radiol. 98 (2018) 187–192.

[4] T. Tamada, A. Kido, M. Takeuchi, A. Yamamoto, Y. Miyaji, N. Kanomata, T. Sone, Comparison of PI-RADS version 2 and PI-RADS version 2.1 for the detection of transition zone prostate cancer, Eur. J. Radiol. 121 (2019), 108704.

[5] L. Zhang, M. Tang, S. Chen, X. Lei, X. Zhang, Y. Huan, A meta-analysis of use of prostate imaging reporting and data system version 2 (PI-RADS V2) with multiparametric MR imaging for the detection of prostate cancer, Eur. Radiol. 27 (12) (2017) 5204–5214.

[6] H.U. Ahmed, A. El-Shater Bosaily, L.C. Brown, R. Gabe, R. Kaplan, M.K. Parmar, Y. Collaco-Moraes, K. Ward, R.G. Hindley, A. Freeman, A.P. Kirkham, R. Oldroyd, C. Parker, M. Emberton, P.s. group, Diagnostic accuracy of multi-parametric MRI and TRUS biopsy in prostate cancer (PROMIS): a paired validating confirmatory study, Lancet 389 (10071) (2017) 815–822.

[7] V. Kasivisvanathan, A.S. Rannikko, M. Borghi, V. Panebianco, L.A. Mynderse, M. H. Vaarala, A. Briganti, L. Budaus, G. Hellawell, R.G. Hindley, M.J. Roobol, S. Eggener, M. Ghei, A. Villers, F. Bladou, G.M. Villeirs, J. Virdi, S. Boxler, G. Robert, P.B. Singh, W. Venderink, B.A. Hadaschik, A. Ruffion, J.C. Hu, D. Margolis, S. Crouzet, L. Klotz, S.S. Taneja, P. Pinto, I. Gill, C. Allen, F. Giganti, A. Freeman, S. Morris, S. Punwani, N.R. Williams, C. Brew-Graves, J. Deeks, Y. Takwoingi, M. Emberton, C.M. Moore, P.S.G. Collaborators, MRI-targeted or standard biopsy for prostate-cancer diagnosis, N. Engl. J. Med. 378 (19) (2018) 1767–1777.

[8] M.R. Pokorny, M. de Rooij, E. Duncan, F.H. Schroder, R. Parkinson, J.O. Barentsz, L.C. Thompson, Prospective study of diagnostic accuracy comparing prostate cancer detection by transrectal ultrasound-guided biopsy versus magnetic resonance (MR) imaging with subsequent MR-guided biopsy in men without previous prostate biopsies, Eur. Urol. 66 (1) (2014) 22–29.

[9] T. Ullrich, C. Arsov, M. Quentin, N. Laqua, M. Klingebiel, O. Martin, A. Hiester, D. Blondin, R. Rabenalt, P. Albers, G. Antoch, L. Schimmoller, Analysis of PI-RADS 4 cases: management recommendations for negatively biopsied patients, Eur. J. Radiol. 113 (2019) 1–6.

[10] American College of Radiology, PI-RADS, Prostate Imaging-Reporting and Data System Version 2, 2015 http://www.acr.org/~/media/ACR/Documents/PDF/QualitySafety/Resources/PIRADS/PIRADS%20V2.pdf/ (Accessed 24 March 2018).

[11] B.K. Barth, A. Cornelius, D. Nanz, D. Eberli, O.F. Donati, Comparison of image quality and patient discomfort in prostate MRI: pelvic phased array coil vs. Endorectal coil, Abdom. Radiol. (NY) 41 (11) (2016) 2218–2226.

[12] A.D. Baur, T. Daqqaq, M. Wagner, A. Maxeiner, A. Huppertz, D. Renz, B. Hamm, T. Fischer, T. Durmus, T2- and diffusion-weighted magnetic resonance imaging at 3T for the detection of prostate cancer with and without endorectal coil: an intraindividual comparison of image quality and diagnostic performance, Eur. J. Radiol. 85 (6) (2016) 1075–1084.

[13] M. Baldisserotto, E.J. Neto, G. Carvalhal, A.F. de Toledo, C.M. de Almeida, C. E. Cairoli, D.O. de Silva, E. Carvalhal, R.P. Paganin, A. Agra, F.S. de Santos, J. A. Noronha, Validation of PI-RADS v.2 for prostate cancer diagnosis with MRI at 3T using an external phased-array coil, J. Magn. Reson. Imaging 44 (5) (2016) 1354–1359.

[14] Y. Mazaheri, D.A. Goldman, P.L. Di Paolo, O. Akin, H. Hricak, Comparison of prostate volume measured by endorectal coil MRI to prostate specimen volume and mass after radical prostatectomy, Acad. Radiol. 22 (5) (2015) 556–562.

[15] B. Turkbey, M.J. Merino, E.C. Gallardo, V. Shah, O. Aras, M. Bernardo, E. Mena, D. Daar, A.R. Rastinehad, W.M. Linehan, B.J. Wood, P.A. Pinto, P.L. Choyke, Comparison of endorectal coil and nonendorectal coil T2W and diffusion-weighted MRI at 3 Tesla for localizing prostate cancer: correlation with whole-mount histopathology, J. Magn. Reson. Imaging 39 (6) (2014) 1443–1448.

[16] J. Weiss, P. Martirosian, M. Notohamiprodjo, S. Kaufmann, A.E. Othman, U. Grosse, K. Nikolaou, S. Gatidis, Implementation of a 5-Minute magnetic resonance imaging screening protocol for prostate Cancer in men with elevated prostate-specific antigen before biopsy, Invest. Radiol. 53 (3) (2018) 186–190.

[17] M.P. McDougall, S.M. Wright, 64-channel array coil for single echo acquisition magnetic resonance imaging, Magn. Reson. Med. 54 (2) (2005) 386–392.

[18] T. Niendorf, C.J. Hardy, R.O. Giaquinto, P. Gross, H.E. Cline, Y. Zhu, G. Kenwood, S. Cohen, A.K. Grant, S. Joshi, N.M. Rofsky, D.K. Sodickson, Toward single breath-hold whole-heart coverage coronary MRA using highly accelerated parallel imaging with a 32-channel MR system, Magn. Reson. Med. 56 (1) (2006) 167–176.

[19] J. Weiss, P. Martirosian, S. Wolf, W. Horger, J. Taron, K. Nikolaou, M. Notohamiprodjo, A.E. Othman, Fast abdominal contrast-enhanced imaging with high parallel-imaging factors using a 60-Channel receiver coil setup: comparison with the standard coil setup, Invest. Radiol. 53 (10) (2018) 602–608.

[20] G.C. Wiggins, J.R. Polimeni, A. Potthast, M. Schmitt, V. Alagappan, L.L. Wald, 96-Channel receive-only head coil for 3 Tesla: design optimization and evaluation, Magn. Reson. Med. 62 (3) (2009) 754–762.

[21] G.C. Wiggins, C. Triantafyllou, A. Potthast, A. Reykowski, M. Nittka, L.L. Wald, 32-channel 3 Tesla receive-only phased-array head coil with soccer-ball element geometry, Magn. Reson. Med. 56 (1) (2006) 216–223.

[22] Y. Zhu, C.J. Hardy, D.K. Sodickson, R.O. Giaquinto, C.L. Dumoulin, G. Kenwood, T. Niendorf, H. Lejay, C.A. McKenzie, M.A. Ohliger, N.M. Rofsky, Highly parallel volumetric imaging with a 32-element RF coil array, Magn. Reson. Med. 52 (4) (2004) 869–877.

[23] S.J. Riederer, E.A. Borisch, A.T. Froemming, R.C. Grimm, A. Kawashima, L. A. Mynderse, J.D. Trzasko, Improved performance of prostate DCE-MRI using a 32-coil vs. 12-coil receiver array, Magn, Reson, Imaging 39 (2017) 15–23.

[24] A. Deshmane, V. Gulani, M.A. Griswold, N. Seiberlich, Parallel MR imaging, J. Magn. Reson. Imaging 36 (1) (2012) 55–72.

[25] O. Dietrich, J.G. Raya, S.B. Reeder, M.F. Reiser, S.O. Schoenberg, Measurement of signal-to-noise ratios in MR images: influence of multichannel coils, parallel imaging, and reconstruction filters, J. Magn. Reson. Imaging 26 (2) (2007) 375–385.
[26] L. Filli, M. Piccirelli, D. Kenkel, R. Guggenberger, G. Andreisek, T. Beck, V. M. Runge, A. Boss, Simultaneous multislice echo planar imaging with blipped controlled aliasing in parallel imaging results in higher acceleration: a promising technique for accelerated diffusion tensor imaging of skeletal muscle, Invest. Radiol. 50 (7) (2015) 456–463.
[27] A. Manoliu, M. Ho, M. Piccirelli, D. Nanz, L. Filli, E. Dappa, W. Liu, D.A. Ettlin, A. Boss, G. Andreisek, F.P. Kuhn, Simultaneous multislice readout-segmented echo planar imaging for accelerated diffusion tensor imaging of the mandibular nerve: a feasibility study, J. Magn. Reson. Imaging 46 (3) (2017) 663–677.
[28] S.B. Reeder, B.J. Wintersperger, O. Dietrich, T. Lanz, A. Greiser, M.F. Reiser, G. M. Glazer, S.O. Schoenberg, Practical approaches to the evaluation of signal-to-noise ratio performance with parallel imaging: application with cardiac imaging and a 32-channel cardiac coil, Magn. Reson. Med. 54 (3) (2005) 748–754.
[29] D. Stocker, A. Manoliu, A.S. Becker, B.K. Barth, D. Nanz, M. Klarhofer, O.F. Donati, Image quality and geometric distortion of modern diffusion-weighted imaging sequences in magnetic resonance imaging of the prostate, Invest. Radiol. 53 (4) (2018) 200–206.
[30] K.A. Hallgren, Computing inter-rater reliability for observational data: an overview and tutorial, Tutor. Quant. Methods Psychol. 8 (1) (2012) 23–34.
[31] A. Fedorov, M.G. Vangel, C.M. Tempany, F.M. Fennessy, Multiparametric magnetic resonance imaging of the prostate: repeatability of volume and apparent diffusion coefficient quantification, Invest. Radiol. 52 (9) (2017) 538–546.
[32] P.B. Roemer, W.A. Edelstein, C.E. Hayes, S.P. Souza, O.M. Mueller, The NMR phased array, Magn. Reson. Med. 16 (2) (1990) 192–225.
[33] J.A. de Zwart, P.J. Ledden, P. van Gelderen, J. Bodurka, R. Chu, J.H. Duyn, Signal-to-noise ratio and parallel imaging performance of a 16-channel receive-only brain coil array at 3.0 Tesla, Magn. Reson. Med. 51 (1) (2004) 22–26.
[34] J. Taron, P. Martirosian, T. Kuestner, N.F. Schwenzer, A. Othman, J. Weiss, M. Notohamiprodjo, K. Nikolaou, C. Schraml, Scan time reduction in diffusion-weighted imaging of the pancreas using a simultaneous multislice technique with different acceleration factors: how fast can we go? Eur. Radiol. 28 (4) (2018) 1504–1511.
[35] J.A. de Zwart, P.J. Ledden, P. Kellman, P. van Gelderen, J.H. Duyn, Design of a SENSE-optimized high-sensitivity MRI receive coil for brain imaging, Magn. Reson. Med. 47 (6) (2002) 1218–1227.
[36] C.J. Hardy, R.O. Giaquinto, J.E. Piel, K.W. Rohling, L. Marinelli, D.J. Blezek, E. W. Fiveland, R.D. Darrow, T.K. Foo, 128-channel body MRI with a flexible high-density receiver-coil array, J. Magn. Reson. Imaging 28 (5) (2008) 1219–1225.
[37] N. Martini, M.F. Santarelli, G. Giovannetti, M. Milanesi, D. De Marchi, V. Positano, L. Landini, Noise correlations and SNR in phased-array MRS, NMR Biomed. 23 (1) (2010) 66–73.
[38] S.M. Wright, L.L. Wald, Theory and application of array coils in MR spectroscopy, NMR Biomed. 10 (8) (1997) 394–410.